International Journal of Biological Macromolecules 109 (2018) 1239–1245

Contents lists available at ScienceDirect

International Journal of Biological Macromolecules

journal homepage: www.elsevier.com/locate/ijbiomac

Crystallinity and lowering band gap induced visible light photocatalytic activity of TiO_2/CS (Chitosan) nanocomposites

R. Saravanan [a,*], J. Aviles [a], F. Gracia [a,*], E. Mosquera [b], Vinod Kumar Gupta [c,d]

[a] Department of Chemical Engineering, Biotechnology and Materials, University of Chile, Beauchef 851 6th floor, Santiago, Chile
[b] Departamento de Física, Universidad del Valle, A.A. 25360, Cali, Colombia
[c] Department of Applied Chemistry, University of Johannesburg, Johannesburg, South Africa
[d] Department of Biological Sciences, Faculty of Science, King Abdulaziz University, Jeddah, Saudi Arabia

ARTICLE INFO

Article history:
Received 28 June 2017
Received in revised form
14 November 2017
Accepted 19 November 2017
Available online 23 November 2017

Keywords:
Photocatalyst
Nanocomposites
Visible light

ABSTRACT

The inhibition of electrons-holes recombination and enhancement of visible light photocatalytic activity were accomplished by the synthesized TiO_2/CS nanocomposites system. In this present work, the different weight ratio of TiO_2 and chitosan (75:25, 50:50 and 25:75) nanocomposites were synthesized via two-step method. After that, the existing functional groups, size and structure of the nanocomposites system were characterized via FT-IR, TEM and XRD measurements. The band gap of the prepared materials and its excitation and emission spectra were elevated through UV–vis and PL analyses. Moreover, the MO and MB degradation capability of the synthesized TiO_2/CS nanocomposites was optimized, and the outcomes are described in detail.

1. Introduction

Worldwide, the elimination of colored effluents is one of the essential issue due to preserving a good eco-friendly nature [1,2]. During the sunlight illumination, the devastation of diverse pollutions from the atmosphere is an imperative and exacting task for the researchers [3,4]. In this connection, addressing and resolving the above problem via photocatalytic method. While comparing with other elimination methods, photocatalyst is a unique advantage like simple and cost-effective approach [5–7]. In the recent times, nanomaterial based catalysts used for several applications [8–16]; especially titanium dioxide (TiO_2) nanomaterial is one of the most conspicuous photocatalysts due to its band position which most favor for the oxidation process during the photocatalytic activity [17]. In nature, the TiO_2 has obtained on three phases containing anatase, rutile, and brookite, the most attractive and sensitive phase is anatase because of extraordinary photocatalytic activity while associated with the other two phases. The main inadequacy of anatase phase is it generated electrons and holes only under UV light irradiation. For the period of the photocatalytic activity, the generation and prevention of electrons and holes are crucial to achieve a higher degradation rate [3,6,17].

In this present work, the key impartial is a visible light degradation of colored dyes. For the purpose, it needs TiO_2 material shine to absorb solar spectrum. The alteration of TiO_2 material is an indispensable way to absorb visible light. The accumulation or doping with metal/non-metal/composite structure contributes in-between band state or disordering the band structure of TiO_2 which is favorable and offering the ability of TiO_2 to absorb solar irradiation and generates more electron and holes under visible light condition [3,6,17,18]. On the other hand, beside of TiO_2 with nature bio polymers (cellulose, chitosan etc.,) is a simplest and safest way to attain visible light degradation [19–22]. Among other natural polymers, chitosan contains amino and hydroxyl groups. These groups are more service to accomplish the degradation of effluents [21,22].

In this present work, various weight percentages of chitosan-TiO_2 nanocomposite materials were prepared by sol-gel followed by precipitation method. The structural, morphological and optical properties were characterized by X-ray diffraction (XRD), transmission electron microscopy (TEM), Fourier transform infrared (FT-IR), photoluminescence (PL) and UV–vis absorption (UV–vis) spectroscopic studies. Additionally, the synthesized catalysts were used to degrade methyl orange (MO) and methylene blue (MB) solution by photocatalytic processes under visible light condition.

* Corresponding authors at: Department of Chemical Engineering, Biotechnology and Materials, University of Chile, Beauchef 851 6th floor, Santiago, Chile
E-mail addresses: saravanan3.raj@gmail.com (R. Saravanan), fgracia@ing.uchile.cl (F. Gracia).

https://doi.org/10.1016/j.ijbiomac.2017.11.125
0141-8130/

2. Experimental

2.1. Materials

Titanium tetra isopropoxide (TTIP, $C_{12}H_{28}O_4Ti$, Sigma Aldrich 97%), acetic acid (CH_3COOH, ≥99.7%), isopropanol (C_3H_8O, ≥99.5%), Chitosan (CS, Sigma Aldrich, 75–85%) and deionized water are essential to synthesis of pure TiO_2 and TiO_2/Chitosan (TiO2/CS) nanocomposites. For Photocatalytic test, we have used methyl orange and methylene blue (Sigma Aldrich) as a model dye.

2.2. Synthesis of TiO_2 nanoparticles

The real synthesis process of titania nanoparticles via sol-gel method followed by the previous report [23]. In this process, to begin with 1:2 ratio of acetic acid is mixed with an isopropanol solution under persistent stirring condition (600 RPM) around ~1 h. Then, 25 mL of TTIP solution was instantly transferred to the above stirring mixed solution and permitted to react for an additional 30 min. As a final step, 17.5 mL of deionized water is added to the above-stirred solution. It was clearly seen in this stage; the solution was completely transformed into gel mode and the gel was permitted to dry at 150 °C for 1 h to get amorphous TiO_2 powder materials. To end, the amorphous TiO_2 material was totally reformed into anatase crystalline nature at 400° C for 1 h.

2.3. Synthesis of TiO_2/CS nanocomposites

The different weight proportion (75:25, 50:50 and 25:75) of TiO_2/CS photocatalysts were synthesized by the two-step method. At first, we have prepared TiO_2 nanoparticles by the sol-gel method. For the second step, different masses of TiO_2 and chitosan (75:25, 50:50 and 25:75) were measured. The mixed (TiO_2 and chitosan) powder was dissolved 20 mL of acetic acid (≥99.7%) with constant stirring for ~25 to 30 min. The pH of the above dissolved solution was adjusted by NaOH solution due to get precipitation of mixed powder. Consequently, the precipitated powder was placed in an ultrasonic bath for one hour because of reduction of the size of the nanocomposites. At that point, the solution was centrifuged (10,000 RPM for 15 min) to separate and recovered the nanocomposite solid phase. Then, the nanocomposite powder was collected and dried on a Petri dish at 50–55° C for 12 h. The synthesized photocatalysts were named according to the nomenclature TiO_2/CS (75:25), TiO_2/CS (50:50) and TiO_2/CS (25:75).

2.4. Photocatalytic activity testing procedure

The core impartial of the existing work is visible light photocatalytic activity. In this association, the synthesized materials were meritoriously exploited for the degradation of MO and MB dye. The testing procedure of photocatalytic activity was described in our earlier reports [24–28]. In the beginning, the photoreaction was arranged by the combination of catalyst (100 mg) along with MO and MB dye solution (5×10^{-5} mol/L). During the photocatalytic reaction, the whole reaction temperature was sustained at 25 °C. The solar simulator (SCIENCETECH, model no: SF300 B along with AM 1.5G filter) was used as a visible light source. At a consistent interval of time, the combined stirring solution was exposed by the solar simulator and it was collected. The absorption significance of unexposed and exposed solutions was scrutinized by UV–vis absorption spectrophotometer. The degradation percentage was premeditated by the following equation [24,25]

$$\eta = \left[1 - \frac{C}{C_0}\right] \times 100 \quad (1)$$

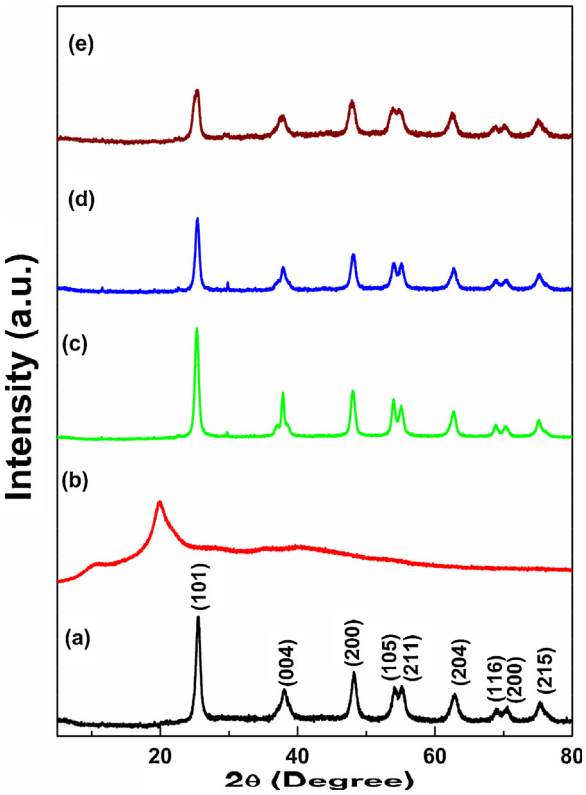

Fig 1. XRD pattern of prepared (a) Pure TiO_2, (b) Chitosan, (c) TiO_2/CS (75:25), (d) TiO_2/CS (50:50), and (**e**) TiO_2/CS (25:75).

Where, η is the degradation efficiency, C_0 and C are the absorption value of the dye solution before exposed (t = 0) and after exposed light for 't' minutes correspondingly.

2.5. Characterization details

The phase purity and crystallite size of the synthesized catalysts were scrutinized via XRD measurement (D5000 diffractometer, Siemens, USA) at room temperature. From the transmission electron microscopic (Tecnai F20-FEI, USA) analysis, we have to find particle shape and size of the prepared materials. The excitation wavelength, band gap (from Tauc plot) and absorption value of the degradation solutions were investigated by a UV–visible spectrophotometer (Perkin Elmer Lambda 35, USA). The emission spectra of the prepared materials were established by photoluminescence (Perkin Elmer spectrofluorometer LS-55) with an excitation wavelength 410 nm.

3. Results and discussion

The X-ray diffraction patterns of synthesized three TiO_2/CS (75:25, 50:50 and 25:75) nanocomposite samples, in addition to pure TiO_2 and chitosan results were exposed in Fig. 1. The XRD outcome of pure TiO_2 is diffraction peaks observed at 2θ values of 25.51°, 38.18°, 48.12°, 53.89°, 55.17°; 62.87°; 68.97°; 70.56° and 75.46° which is correspond to the tetragonal anatase crystalline phase and their matching *hkl* planes (1 0 1), (0 4), (2 0), (1 0 5), (2 1), (2 0 4), (1 6), (2 0) and (2 1 5) respectively. The entire TiO_2 diffraction pattern was related with standard JCPDS No 21–1272. On the other hand, the pure chitosan shows two major characteristic peaks for 2θ of 10.62° and 19.94°. However, small additional peaks were presented around the 28.23°, 35.97° and 40.00°. This similar consequence is consistent with the previous report [29]. For the prepared TiO_2/CS (75:25) sample, the diffraction peaks were detected at the

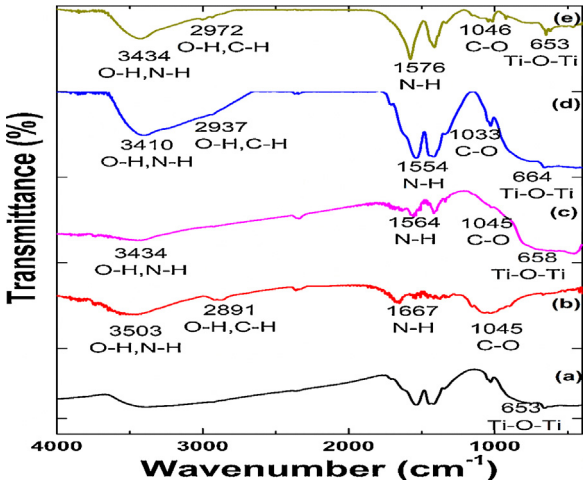

Fig. 2. FT-IR spectra of (a) Pure TiO_2, (b) Chitosan, (c) TiO_2/CS (75:25), (d) TiO_2/CS (50:50), and (**e**) TiO_2/CS (25:75).

2θ values of 25.32°; 29.67°; 37.86°; 47.97°; 53.93°; 55.14°; 62.72°; 68.83°; 70.32° and 75.08°. All the 2θ values are associated with anatase phase of TiO_2 material, excluding the peak at 29.67° which is interrelated with chitosan. The presence of chitosan doesn't alteration of the tetragonal structure of TiO_2. Therefore, the XRD results confirm the formation of the TiO_2/CS nanocomposite system. Likewise, the diffraction pattern of TiO_2/CS (50:50) and TiO_2/CS (25:75) materials were exposed the tetragonal structure of TiO_2 along with chitosan.

For a close examination of the XRD outcomes, the quantity of chitosan content (25, 50 and 75) increases in the nanocomposite system, the intensity of the diffraction peaks decreases. Concurrently, the peak broadening increase. The above declaration was symbolized that the crystallite size was decreasing with increasing chitosan content. Which was substantiated via Scherrer formula (D).

$$D = \frac{K.\lambda}{\beta.cos\left(\theta\right)} \quad (2)$$

Where; D: Average crystalline size [nm], K: Shape Factor, λ: Wavelength of X-rays [Å], β: Corresponds to the full-width half maximum of the diffraction peak [Rad], and θ: Bragg Angle. [°].

The estimated crystallite size was presented in Table 1 and the results were unmistakable covenant the above statement. Hence, the XRD results were unmistakably symbolized the formation of composites is in nano scale range.

The incorporation of chitosan into the TiO_2 matrix was recognized by FT-IR spectra. In Fig. 2 was denoted FT-IR spectra of the different weight percentage of synthesized TiO_2/CS nanocomposites compared with the pure chitosan and TiO_2 compounds. In the spectrum of the pure TiO_2 sample, there is a stretching vibration around 653 cm^{-1} corresponding to Ti-O-Ti bonds. In the case of pure chitosan spectrum, the OH bond is found around 3450 cm^{-1}. Another functional group is around 1045 cm^{-1} which are associated with C—O group [29,30]. Moreover, the chitosan contains

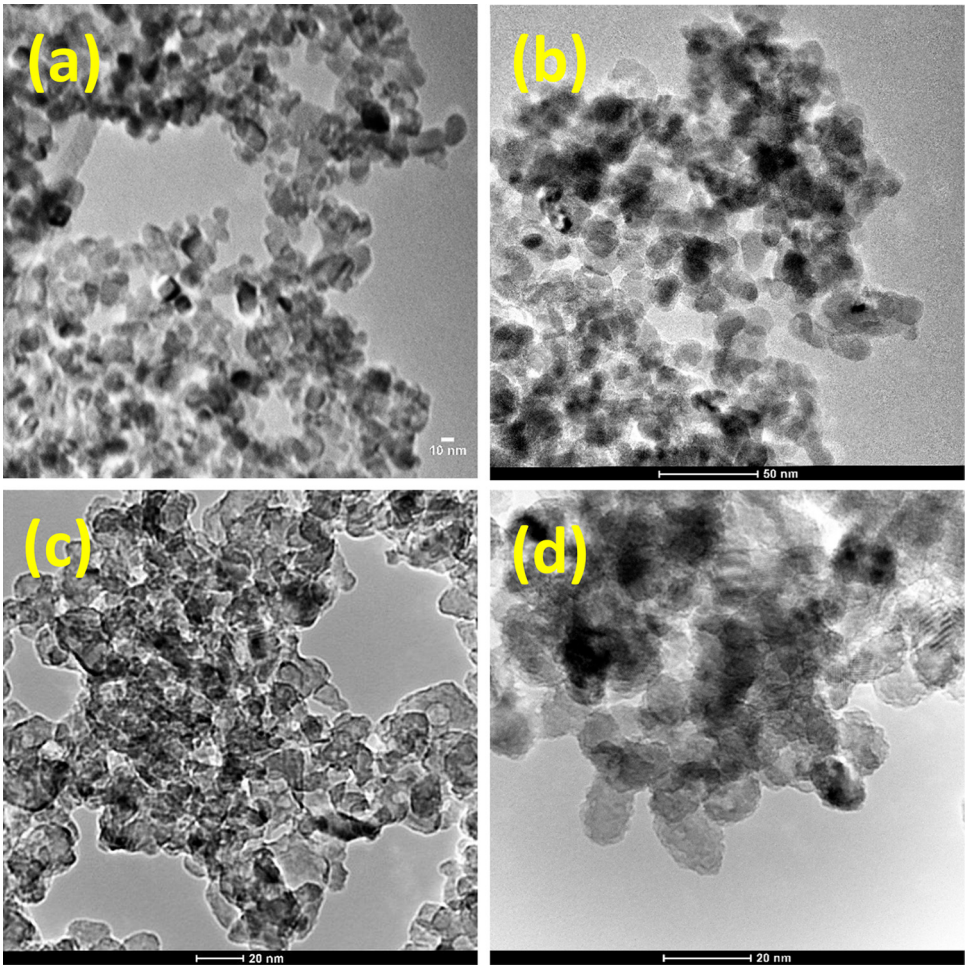

Fig. 3. TEM images of (a) Pure TiO_2, (b) TiO_2/CS (75:25), (c) TiO_2/CS (50:50), and (d) TiO_2/CS (25:75).

Table 1
Band gap, Crystallite and particles size of the prepared materials.

Samples	Band Gap calculated from Tauc Plot E_g (eV)	Crystallite size calculated from Scherrer formula D (nm)	Particle size calculated from particle size distribution based on TEM images (nm)
TiO_2	3.20	14.2	12
TiO_2/CS (75:25)	3.00	11.5	10
TiO_2/CS (50:50)	3.05	10.2	Agglomeration
TiO_2/CS (75:25)	3.13	9.7	Agglomeration

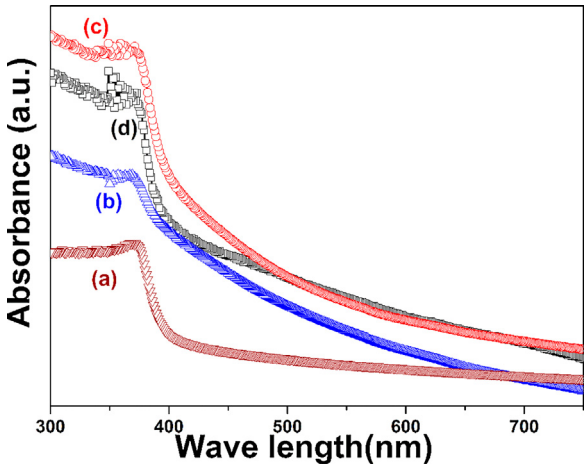

Fig. 4. UV–vis spectra of (a) Pure TiO_2, (b) TiO_2/CS (75:25), (c) TiO_2/CS (50:50), and (d) TiO_2/CS (25:75).

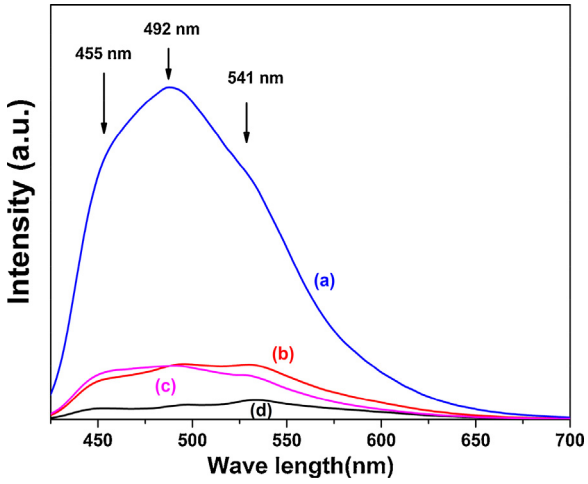

Fig. 5. PL emission spectra of (a) Pure TiO_2, (b) TiO_2/CS (75:25), (c) TiO_2/CS (50:50), and (d) TiO_2/CS (25:75).

amino group which was presented around 1667 cm^{-1}. The survival of hydroxyl and C—H groups (3503 cm^{-1} and 2891 cm^{-1}) were realized in the pure chitosan spectrum [30,31]. After the addition of chitosan, the stretching vibration of C—O, amino and hydroxyl groups relate to the Ti-O-Ti bonds that signified chitosan particles are strongly attached to the TiO_2 materials which authorized the formation TiO_2/CS nanocomposite system [30,31].

The morphology of the prepared pure TiO_2 and different quantity (75:25, 50:50 and 25:75) of TiO_2/CS nanocomposites were explored via TEM instrument. The TEM image of pure TiO_2 shown in Fig. 3a, it was implied spherical fashioned fine nanoparticles and their parallel particle size distribution curve was revealed the particle size value is presented in Table 1.

Subsequently, the content of chitosan increases into TiO_2 matrix, the perfect fine particles were transformed into a combined group of particles. The calculated particle size of the nanocomposite materials was tabularized in Table 1. The increasing chitosan (50 and 75 wt ratios) was the complete destruction of the TiO_2 surface (visibly realized in Fig. 3c and d) which implies that the chitosan particles are spread over on the TiO_2 matrix. Therefore, the TEM images were suggested that the higher amount chitosan content (50 and 75 wt ratios) decreases the crystallinity of the TiO_2 nanoparticles. Moreover, the XRD results were authorized the similar observation

The fundamental parameters of photocatalytic activity primarily depend on the wavelength of the exposed light and bandgap of the synthesized materials which were recognized by UV–vis absorption spectra. In Fig. 4 indicates the UV–vis absorption spectra of pure TiO_2 and TiO_2/CS (75:25, 50:50 and 25:75) nanocomposites.

From the spectra, the absorption power of TiO_2/CS (75:25, 50:50 and 25:75) is in the red area which conveys that the nanocomposites absorb or active in the visible light due to the existence of chitosan into TiO_2 matrix which leads the absorption edge in visible range. Meanwhile, the absorption power of pure TiO_2 is in the blue area. Kang et al. recently identified that the amorphous or semi-crystalline material was showing the absorption edge in wider range, whereas the crystallite material has very sharp edge [32]. In our case, the nanocomposite materials were displayed semi-crystalline nature. In the interim, the pure TiO_2 material shows well crystalline property. The XRD outcome was endorsed the above declaration. The band gap of the prepared samples was obtained by Tauc plots, the below formula was connected the absorbance edges of the sample to the energy of the incident photons [33].

$$\alpha.h.\nu = A(h.\nu - E_g)^n \quad (3)$$

Where α = absorbance value is attained from the spectra, h = Planck's constant, $\nu = c/\lambda$, ν = frequency of the incident wave, c = velocity of light and λ = wavelength acquired from the spectra. A = constant. Eg: energy gap between the valence and conduction bands, and n = parameter associated with the electronic transition. In our case, indirect semiconductors n = ½. The Tauc plot of the synthesized materials was displayed in Fig. S1 (supplementary information) and the determined values are listed in Table 1. The result was clearly embodied that after the addition of chitosan, the bandgap value decreases gradually. Which leads to use the prepared composites for the photocatalytic removal of MO dye under the visible irradiation.

The electrons-holes recombination process of the synthesized pure TiO_2 and TiO_2/CS nanocomposite materials were identified by photoluminescence (PL) spectroscopy with an excitation wavelength is 410 nm. The PL emission spectra were presented in Fig. 5 and their conforming lead band transitions seemed at 455 nm, 492 nm and 541 nm which symbolized the occurrence of anatase phase TiO_2 material [34–36].

Additionally, the emission intensities of the nanocomposites system were dropped. Conversely, the pure TiO_2 material displays fast recombination so the intensity is higher than that of TiO_2/CS nanocomposite system. We know that the dropping emission intensities stated that hindrance of electrons-holes recombination

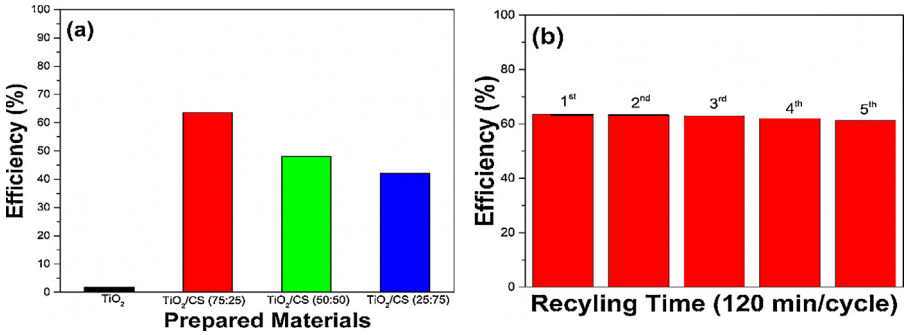

Fig. 6. (**a**) Photocatalytic degradation efficiency of all prepared materials against MO dye and (**b**) Recycling ability of TiO_2/CS (75:25) against MO dye.

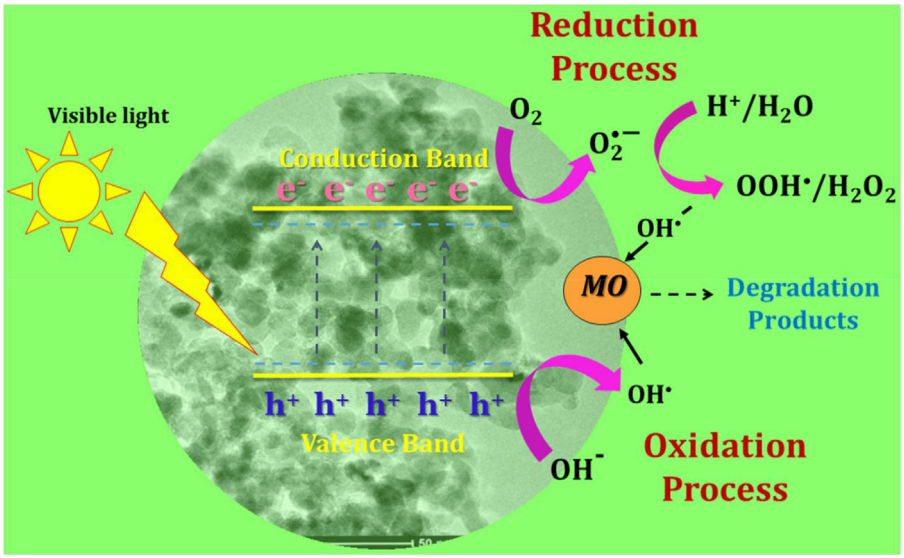

Fig. 7. Photocatalytic mechanism of TiO_2/CS nanocomposite system.

process, which is extremely preferential for an enrichment of the photocatalytic degradation reaction [34–36].

3.1. Photocatalytic evaluation

The primary objective of the existing work is to an evaluation of the degradation capacity of the prepared nanocomposites system under the solar simulator (visible light) condition, MO dye was used for degradation purpose because this dye commonly used for several textile industries moreover very strong stability under solar irradiation. Initially, an organized photolysis (without catalyst) investigation was performed and their outcomes displayed that MO dye having good stability under the illumination. Preliminary (without illumination) and light up or irradiated dye solutions were collected in a vial at every 20-min period. After the 120 min of exposed of light, the absorption value of the solutions was monitored by UV–vis absorption spectra and the efficiency results (Fig. 6a) was evidently revealed that pure titania is not able to degrade the MO solution and value is lower because of its large bandgap. Rest of the nanocomposite samples were shown improved efficiency against MO and reaching (within 120 min) 63.58%, 48.08% and 42.08% efficiencies for TiO_2/CS (75:25), TiO_2/CS (50:50) and TiO_2/CS (25:75) respectively and the enhanced efficiency because of the nanocomposite contains chitosan. The amino and hydroxyl groups are favor of better degradation efficiencies under solar irradiation [25,37,38] Associated with other TiO_2/CS (50:50) and TiO_2/CS (25:75) nanocomposite systems, the TiO_2/CS (75:25) exposed superior efficiency due to good crystallinity and lower bandgap. Recently Gupta et al. defined that the crystallinity of the material plays an active role to attained better degradation rate [25].

The nanocomposite TiO_2/CS (75:25) photocatalyst was shown respect and comparable efficiencies against related similar systems in Table S1 (supplementary information) for the removal of colored and colorless discharges such as methylene blue, permethrin, methyl orange and phenolic compounds under UV and sun light [25,29,37,39–42], and MO degradation [25,29,37]. The present work suggests that TiO_2/CS (75:25) material displayed significant a rate improvement for MO photodegradation (63.58% within 120 min under visible light). Besides, the MO degradation results were equated with the degradation rates of MB (Fig. S2, supplementary information). The degradation percentage of MB is high while comparable with MO results due to its structure [24,25]. Moreover, the recycling outcomes (Fig. 6b) of TiO_2/CS (75:25), authorized that the prepared nanocomposite catalyst was displayed a strong and stable performance (after 5 times) against MO under similar condition.

The beginning of the photocatalytic reaction, when solar irradiation reached on the nanocomposite surface, the valence band electrons are gripped the solar irradiation or photons and eagerly transfer into the conduction band of the system. The voids or holes remain in the valence band. The period of a photocatalytic process, the number of electrons and holes are produced by nanocomposite system because its small bandgap is highly favored for visible light absorption [24–28]. On the other side, their intermediate states provided the struggle or delay of electrons-holes recombination

[24,25,29]. The subsequent equation and diagram (Fig. 7) were clearly signified the photocatalytic mechanism [43–45].

$$TiO_2/CS + h\nu \rightarrow TiO_2/CS\left(e^-_{BC}\right) + TiO_2/CS\left(h^+_{BV}\right) \quad (4)$$

$$TiO_2/CS\left(h^+_{BV}\right) + H_2O \rightarrow TiO_2/CS + H^+ + OH^\bullet \quad (5)$$

$$TiO_2/CS\left(e^-_{BC}\right) + O_2 \rightarrow TiO_2/CS + O_2^{\bullet -} \quad (6)$$

$$O_2^{\bullet -} + H^+ \rightarrow OOH^\bullet \quad (7)$$

$$O_2^{\bullet -} + H_2O \rightarrow OOH^\bullet + OH^- \quad (8)$$

$$OOH^\bullet + H^+ + TiO_2/CS\left(e^-_{BC}\right) \rightarrow H_2O_2 + TiO_2/CS \quad (9)$$

$$OOH^\bullet + H_2O + TiO_2/CS\left(e^-_{BC}\right) \rightarrow H_2O_2 + OH^- + TiO_2/CS \quad (10)$$

$$H_2O_2 + TiO_2/CS\left(e^-_{BC}\right) \rightarrow OH^\bullet + OH^- + TiO_2/CS \quad (11)$$

$$H_2O_2 + OH^- \rightarrow OH^\bullet + OH^- \quad (12)$$

$$H_2O_2 + h\nu \rightarrow 2OH^\bullet \quad (13)$$

$$OH^\bullet + MO\ dye \rightarrow Degradation\ product \quad (14)$$

Finally in short, the conduction band electrons and valence band holes react with water molecules (presented in the MO dye) and tempted oxidation and reduction process respectively. Both reactions, highly produced OH radicals, which was effectively destroyed the MO structure.

4. Conclusion

In this present work, we are successfully prepared different weight percentage of TiO_2/CS nanocomposites via sol-gel followed precipitation method. After the addition of chitosan, the TiO_2 material not change their own tetragonal structure. But concurrently the increases of chitosan contents (50 and 75 wt ratios), reduce the crystallinity of the TiO_2 materials which was established by XRD and TEM measurements. In the nanocomposites contains amino and hydroxyl groups which was favored to attain visible light photocatalytic activity. While paralleling with pure and other prepared nanocomposites, the TiO_2/CS (75:25) material showing greater degradation efficiency against MO dye due to its good crystallinity and lowering bandgap. Moreover, the recycling outcome of TiO_2/CS (75:25) material shows effective stability. Therefore, the TiO_2/CS (75:25) was excellently used for long term environmental catalysts against textile effluents.

Acknowledgement

The authors (S.R., F.G.) acknowledge the support of CONICYT through the project CONICYT/FONDECYT/3150631 and the postdoctoral fellowship granted to S.R. The author (F.G.) acknowledge the support of CONICYT through the project CONICYT/FONDAP/15110019.

References

[1] J. Kou, et al., Selectivity enhancement in heterogeneous photocatalytic transformations, Chem. Rev. 117 (3) (2017) 1445–1514.
[2] M. Rochkind, S. Pasternak, Y. Paz, Using dyes for evaluating photocatalytic properties: a critical review, Molecules 20 (2015) 88–110.
[3] M. Pelaez, et al., A review on the visible light active titanium dioxide photocatalysts for environmental applications, Appl. Catal. B: Environ. 125 (2012) 331–349.
[4] L. Mohapatra, K. Parida, A review of solar and visible light active oxo-bridged materials for energy and environment, Catal. Sci. Technol. 7 (2017) 2153–2164.
[5] D.Y. Wan, et al., Electron transport and visible light absorption in a plasmonic photocatalyst based on strontium niobate, Nat. Commun. 8 (2017) 15070.
[6] K.M. Reza, A.S.W. Kurny, F. Gulshan, Parameters affecting the photocatalytic degradation of dyes using TiO2: a review, Appl. Water Sci. 7 (4) (2017) 1569–1578.
[7] A. Fujishima, K. Honda, Electrochemical photolysis of water at a semiconductor electrode, Nature 238 (1972) 37–38.
[8] S. Cheraghi, M.A. Taher, H.K. Maleh, Highly sensitive square wave voltammetric sensor employing CdO/SWCNTs and room temperature ionic liquid for analysis of vanillin and folic acid in food samples, J. Food Compos. Anal. 62 (2017) 254–259.
[9] H.K. Maleh, F. Amini, A. Akbari, M. Shojaei, Amplified electrochemical sensor employing CuO/SWCNTs and 1-butyl-3-methylimidazolium hexafluorophosphate for selective analysis of sulfisoxazole in the presence of folic acid, J. Colloid Interface Sci. 495 (2017) 61–67.
[10] F.T. Javazmi, M.S. Nooshabadi, H.K. Maleh, Analysis of glutathione in the presence of acetaminophen and tyrosine via an amplified electrode with MgO/SWCNTs as a sensor in the hemolyzed erythrocyte, Talanta 176 (2018) 208–213.
[11] H.K. Maleh, et al., Simultaneous determination of 6-mercaptopruine, 6-thioguanine and dasatinib as three important anticancer drugs using nanostructure voltammetric sensor employing Pt/MWCNTs and 1-butyl-3-methylimidazolium hexafluoro phosphate, Biosens. Bioelectron. 86 (2016) 879–884.
[12] P. Dhiman, M. Naushad, K.M. Batoo, A. Kumar, G. Sharma, A.A. Ghfar, G. Kumar, M. Singh, Nano FexZn1-xO as a tuneable and efficient photocatalyst for solar powered degradation of bisphenol A from aqueous environment, J. Cleaner Prod. 165 (2017) 1542–1556.
[13] A. Kumar, M. Naushad, A. Rana, G. Sharma, A.A. Ghfar, F.J. Stadler, M.R. Khan, ZnSe-WO3 nano-hetero-assembly stacked on Gum Ghatti for photo-degradative removal of Bisphenol A: Symbiose of adsorption and photocatalysis, Intern. J. Biolog. Macromol. 104 (2017) 1172–1184.
[14] D. Pathania, R. Katwal, G. Sharma, Mu. Naushad, M.R. Khan, A.H. ALMuhtaseb, Novel guar gum/Al2O3 nanocomposite as an effective photocatalyst for the degradation of malachite green dye, Intern. J. Biolog. Macromol. 87 (2016) 366–374.
[15] A. Kumar, Shalini Sharma, G. Naushad, M. Kumar, A. Kalia, S. Guo, G.T. Mola, Facile hetero-assembly of superparamagnetic Fe3O4/BiVO4 stacked on biochar for solar photo-degradation of methyl paraben and pesticide removal from soil, J. Photochem. Photobiology A: Chem. 337 (2017) 118–131.
[16] D. Pathania, D. Gupta, A.H. Al-Muhtaseb, G. Sharma, A. Kumar, M. Naushad, T. Ahamad, S.M. Alshehri, Photocatalytic degradation of highly toxic dyes using chitosan-g poly(acrylamide)/ZnS in presence of solar irradiation, J. Photochem. Photobiol. A: Chem. 329 (2016) 61–68.
[17] J. Schneider, et al., Understanding TiO2 photocatalysis: mechanisms and materials, Chem. Rev. 114 (19) (2014) 9919–9986.
[18] V. Etacheri, C.D. Valentin, J. Schneider, D. Bahnemann, S.C. Pillai, Visible-light activation of TiO2 photocatalysts: advances in theory and experiments, J. Photochem. Photobiol. C: Photochem. Rev. 25 (2015) 1–29.
[19] J. Zeng, S. Liu, J. Cai, L. Zhang, TiO2 immobilized in cellulose matrix for photocatalytic degradation of phenol under weak UV light irradiation, J. Phys. Chem. C 114 (17) (2010) 7806–7811.
[21] N.A. Abdelwahab, F.M. Helaly, Simulated visible light photocatalytic degradation of Congo red by TiO2 coated magnetic polyacrylamide grafted carboxymethylated chitosan, J. Ind. Eng. Chem. 50 (2017) 162–171.
[22] A.V. Raut, H.M. Yadav, A. Gnanamani, S. Pushpavanam, S.H. Pawar, Synthesis and characterization of chitosan-TiO2:Cu nanocomposite and their enhanced antimicrobial activity with visible light, Colloids Surf. B: Biointerfaces 148 (2016) 566–575.
[23] T. Prakash, S. Ramasamy, B.S. Murty, Influence of bias voltage on dielectric relaxation of nanocrystalline anatase TiO2 using modulus formalism, J. Appl. Phys. 109 (2011) 084116.
[24] R. Saravanan, E. Sacari, F. Gracia, M.M. Khan, E. Mosquera, V.K. Gupta, Conducting PANI stimulated ZnO system for visible light photocatalytic degradation of colour dyes, J. Mol. Liquids 221 (2016) 1029–1033.
[25] V.K. Gupta, et al., Degradation of azo dyes under different wavelengths of UV light with chitosan-SnO2 nanocomposites, J. Mol. Liquids 232 (2017) 423–430.
[26] R. Saravanan, et al., ZnO/Ag/Mn2O3 nanocomposite for visible light-induced industrial textile effluent degradation, uric acid and ascorbic acid sensing and antimicrobial activities, RSC Adv. 5 (2015) 34645–34651.
[27] R. Saravanan, et al., Enhanced photocatalytic activity of ZnO/CuO nanocomposites for the degradation of textile dye on visible light illumination, Mater. Sci. Eng. C 33 (2013) 91–98.
[28] R. Saravanan, H. Shankar, T. Prakash, V. Narayanan, A. Stephen, ZnO/CdO composite nanorods for photocatalytic degradation of methylene blue under visible light, Mater. Chem. Phys. 125 (2011) 277–280.
[29] H. Zhu, et al., Effective photocatalytic decolorization of methyl orange utilizing TiO2/ZnO/chitosan nanocomposite films under simulated solar irradiation, Desalination 286 (2012) 41–48.
[30] M.A. Nawi, A.H. Jawad, S. Sabar, W.S.W. Ngah, Immbolized bilayer of TiO2/Chitosan system for the removal of phenol under irradiation by a 45 watt compact fluorescent lamp, Desalination 280 (2011) 288–296.
[31] Q. Li, H. Su, T. Tan, Synthesis of ion-imprinted chitosan-TiO2 adsorbent and its multi-functional performances, Biochem. Eng. J. 38 (2008) 212–218.
[32] Y. Kang, et al., An amorphous carbon nitride photocatalyst with greatly extended visible-light-responsive range for photocatalytic hydrogen generation, Adv. Mater. 27 (2015) 4572–4577.
[33] B.D. Viezbicke, S. Patel, B.E. Davis, D.P. Birnie lll, Evaluation of the Tauc method for optical absorption edge determination: znO thin films as a model system, Physica Status Solidi B 252 (2015) 1700–1710.

[34] N.F. Jaafar, et al., Direct in situ activation of Ag0 nanoparticles in synthesis of Ag/TiO2 and its photoactivity, Appl. Surf. Sci. 338 (2015) 75–84.
[35] S. Wang, et al., Facile one-pot synthesis of uniform TiO2–Ag hybrid hollow spheres with enhanced photocatalytic activity, Dalton Trans. 42 (2013) 1122–1128.
[36] C. Mercado, Z. Seeley, A. Bandyopadhyay, S. Bose, J.L. McHale, Photoluminescence of dense nanocrystalline titanium dioxide thin films: effect of doping and thickness and relation to gas sensing, ACS Appl. Mater. Interfaces 3 (2011) 2281–2288.
[37] G. Xiao, H. Su, T. Tan, Synthesis of core–shell bioaffinity chitosan–TiO2 composite and its environmental applications, J. Hazard. Mater. 283 (2015) 888–896.
[38] P. Chen, L. Zhu, S. Fang, C. Wang, G. Shan, Photocatalytic degradation efficiency and mechanism of microcystin-RR by mesoporous Bi2WO6 under near ultraviolet light, Environ. Sci. Technol. 46 (4) (2012) 2345–2351.
[39] A.H. Jawad, M.A. Nawi, Oxidation of crosslinked chitosan-epichlorohydrine film and its application with TiO2 for phenol removal, Carbohydr. Polym. 90 (2012) 87–94.
[40] C.E. Zubieta, et al., Reactive dyes remotion by porous TiO2-chitosan materials, J. Hazard. Mater. 152 (2008) 765–777.
[41] S.M. Dehaghi, B. Rahmanifar, A.M. Moradi, P.A. Azar, Removal of permethrin pesticide from water by chitosan–zinc oxide nanoparticles composite as an adsorbent, J. Saudi Chem. Soc. 18 (2014) 348–355.
[42] S. Dhanavel, E.A.K. Nivethaa, V. Narayanan, A. Stephen, Photocatalytic activity of Chitosan/ZnO nanocomposites for degrading methylene blue, Inter. J. ChemTech Res. 6 (3) (2014) 1880–1882.
[43] D.P. Kumar, et al., Synergistic effect of nanocavities in anatase TiO2 nanobelts for photocatalytic degradation of methyl orange dye in aqueous solution, J. Colloid Interface Sci. 477 (2016) 201–208.
[44] M.H. Farzana, S. Meenakshi, Synergistic effect of chitosan and titanium dioxide on the removal of toxic dyes by the photodegradation technique, Ind. Eng. Chem. Res. 53 (1) (2014) 55–63.
[45] M.A. Nawi, S. Sabar, Sheilatina, Photocatalytic decolourisation of Reactive Red 4 dye by an immobilized TiO2/chitosan layer by layer system, J. Colloid Interface Sci. 372 (2012) 80–87.